

Paper submitted to IGARSS '98
for publication in *Proc. IGARSS '98*, Seattle, Washington, 6-10 July, 1998.


Session: Special Invited Session on "Snow and Ice Sheets" (Schedule DD10.08)

Organizer: Dale Winebrenner

General Topic: Remote Sensing of Snow and Ice Sheets

**"Seasat, ERS-1/2 and NSCAT Scatterometer Observed Changes
on the Large Ice Sheets"**

Mark R. Drinkwater
Jet Propulsion Laboratory
California Institute of Technology
4800 Oak Grove Drive
Pasadena, CA 91109, USA

Tel: (818)-354-8189 Fax: (818)-393-6720
email: mrd@pacific.jpl.nasa.gov
URL: <http://oceans-www.jpl.nasa.gov/polar> 

David G. Long
Brigham Young University
Electrical and Computer Engineering Department
459 Clyde Building, Provo, UT 84602, USA

Tel: (801)-378-4383 Fax: (801)-378-6586
email: long@ee.byu.edu

Seasat, ERS-1/2 and NSCAT Scatterometer Observed Changes on the Large Ice Sheets

Mark R. Drinkwater
Jet Propulsion Laboratory, MS 300-323
California Institute of Technology
4800 Oak Grove Drive, CA 91109, USA
Tel: 818-354 8189 Fax: 818-393 6720
Email: mrd@pacific.jpl.nasa.gov
<http://oceans-www.jpl.nasa.gov/polar>

David G. Long
Electrical and Computer Engineering Dept.
Brigham Young University
Provo, UT 84602, USA
Tel: 801-378-4383 Fax: 801-378-6586
Email: long@ee.byu.edu
<http://www.ee.byu.edu/ee/mers>

Abstract - Satellite-borne wind scatterometers are effective tools for monitoring ice sheets and microwave imaging techniques enable comparison of historic and contemporary scatterometer data in climate change studies. We document scattering characteristics of the Greenland ice sheet using data from the NSCAT, ERS-1/2 and Seasat SASS instruments. C- and Ku-band data enable characterization of frequency-dependent scattering characteristics and regional melting delineation. SASS-NSCAT differences show 18 year changes in dry-snow zone extent and indicate the decadal response to changes in the spatial patterns of accumulation and ablation.

INTRODUCTION

Controversy over the relationship between global warming and changes in the Greenland ice sheet [1, 2] make it imperative to accurately quantify mass balance and the time and space scales of variability in snow accumulation and ablation. Briefly in 1978, and since 1991, microwave radar has been used to study relationships between snow and ice surface structure and backscatter characteristics [3, 4]. Using this information radar data is used to map the relative size and locations of ice sheet physical zones or 'facies' [5, 6].

Microwave backscattering depends on both the roughness and physical characteristics of the snow and ice [7, 8]. For example, liquid water in snow dramatically changes the permittivity and thus its scattering signature. This provides an efficient means of monitoring backscatter changes which accompany diagenetic changes occurring due to seasonal ablation and/or metamorphic processes. Synthetic aperture radar (SAR) provides high resolution images of ice sheets, but the spatio-temporal coverage of the 100x100km images is limited. Scatterometers provide comparatively lower resolution but more frequent coverage, and also measure the backscatter coefficient over a broad range of incidence angles [9]. Here we study changes in the Greenland ice sheet using data from NASA's Ku-band scatterometer (NSCAT), the C-band European Space Agency ERS-1 and 2 (EScat) wind scatterometers and the NASA Seasat scatterometer (SASS).

SCATTEROMETER IMAGING OF ICE SHEETS

The June 30, 1997 failure of the Japanese ADEOS I satellite (launched in August 1996), with its NSCAT sensor, resulted in the loss of a valuable tool for ice studies. NSCAT recorded the 14 GHz normalized radar cross-section, σ^0 (hh- and vv-polarized) while crossing the polar regions several times daily. Measurements at various azimuth and incidence angles

were made in hexagonal 25 km resolution cells on a 25 km grid, along two 600 km wide swaths separated by a 400 km wide gap. The Ku-band SASS, from which NSCAT originated, also operated for only three months in 1978 before Seasat failed. It made 50 km resolution measurements along two 500 km swaths on an irregular sampling grid. In contrast, the EScat instruments (launched on ERS-1 in July 1991 and ERS-2 in April 1995) measure σ^0_{vv} along a single 500 km wide swath. EScat acquires 50 km resolution data on a 25 km grid but is switched off during SAR-mode operation.

Over glacial ice, σ^0 (dB) is approximately a linear function of θ in the range $20^\circ \leq \theta \leq 55^\circ$ [5];

$$\sigma^0(\theta) = A + B(\theta - 40^\circ) \quad (1)$$

where the coefficients A and B depend on surface characteristics, polarization, and azimuth angle. A is the 40° 'incidence angle-normalized' backscatter coefficient σ^0 , and B describes its dependence on θ . A and B are both sensitive to snow and ice characteristics. The scatterometer image reconstruction algorithm with filtering (SIRF) is used to generate enhanced resolution images of A and B from scatterometer data from Greenland [5, 9, 10]. Resulting 6-day average images at 3d intervals are a trade-off between resolution enhancement and temporal averaging.

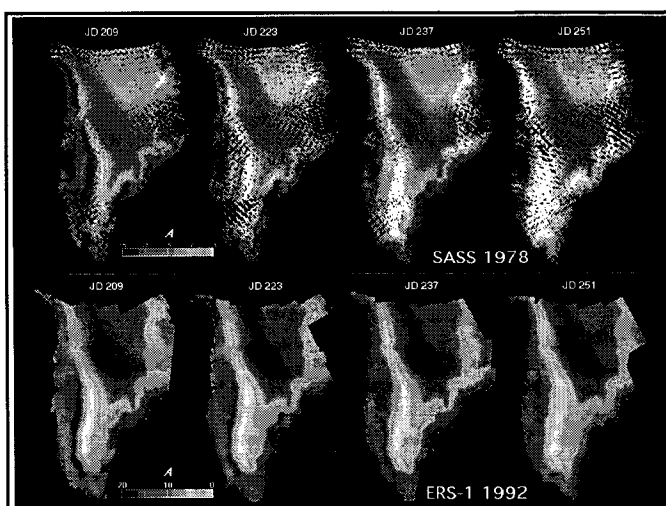


Figure 1. Greenland time series images generated from 1978 SASS and 1992 ERS-1 scatterometer data for selected days of the year. Colors indicate $\sigma^0_{vv}(40^\circ)$ at Ku- and C-band, respectively.

INTERANNUAL ICE SHEET VARIABILITY

The surface of the Greenland ice sheet may be subdivided into 'facies', the boundaries of which are established with respect to extent of melt or ablation influence [6]. Within facies, near-surface snow and ice properties have unique characteristics. At the lowest elevations, summer melting removes the entire annual accumulation of snow to reveal bare glacier ice. The *firn line* delimits the upper margin of this zone, separating it from the 'soaked' facies where saturation of the annual snow layer occurs. The upper limit of soaking is called the *saturation line*. Localized melt-water percolation occurs between this and the upper limit of surface melting, the *dry snow line*. In the 'percolation' facies annual increments of snow are neither completely wetted nor raised to the melting point. Percolation decreases with elevation diminishing to a negligible amount at the lower boundary of the dry snow zone. As glacier facies are not always expressed as strong gradients in surface properties, they are best discerned with microwave measurements which penetrate up to several meters into the surface of the snow and ice [5, 8].

Seasonal modulations of σ° in Fig. 1 indicate changes in surface-layer properties in summer. Meltwater alters the surface reflection or transmissivity, limiting subsurface volume scattering effects by increasing absorption and extinction. In addition, σ° is influenced by layering which results from seasonal snow accumulation and melt patterns [5]. The spatial extent of summer melt appears as low σ°

satellite data record [2], encroaching upslope upon the dry snow zone along the entire north-western ice-sheet flank.

Percolation zone stratigraphic discontinuities and a horizon comprising a high proportion of solid ice in layers, lenses and ice pipes is created as meltwater percolates downwards and refreezes at depth (~1m) [6]. The lower elevation boundary of this zone is clearly indicated in Fig. 1 by a sharp transition between low and extremely high backscatter values. As the surface cools during autumn, the penetration depth increases beyond the depth at which ice lenses form and volume scattering from buried scatterers increases σ° in both Ku- and C-band images to the highest known values on earth [7, 8]. Low σ° values in central Greenland are well separated from percolation zone values exceeding -5 dB. Additionally C-band microwaves penetrate dry snow more effectively than Ku-band. Shorter wavelengths are scattered more effectively by snow grains, and thus the Ku-band σ° exceeds C-band values. Thus, the frequency difference Δ image (*i.e.* EScat-NSCAT) in Fig. 3(e) is used to define the dry-snow line in Fig. 2(a).

Downslope of the firn line, in the saturated facies, horizons are obliterated by the effects of summer melting, reducing winter contrast between the ablation and saturated zones. As a result the two are indistinguishable, and the radar senses only a broad 'ablation zone' [5]. Near the ice sheet margins, the surface autocorrelation function determines A and B by surface scattering, and the roughness scale causes greater backscattering at Ku-band than C-band of up to 8 dB in Fig. 3(e). Together with the seasonal variations in σ° this is used to define the 1996 extent of the ablation zone in Fig. 2a.

DECADAL CHANGE

Acquisition of NSCAT data over the Greenland ice sheet, during the same season as Seasat, enabled long-term change maps to be derived for the period after autumnal cooling. Subtle differences in σ°_{vv} (*i.e.* NSCAT-SASS) between Fig. 3a and b are shown in Fig 3c, (where Fig. 3b is the result of combining and median filtering the sparse SASS measurements). Surfaces experiencing large changes over the intervening 18 year period are in Fig. 3c noted as dark tones with values >3 dB. Patterns appear highly correlated with the snow and ice facies boundaries in Fig. 2a. and the zones of largest interannual variability. The upslope melt extent has a large interannual variability and the mean July melt area in Fig. 2 clearly does not capture the maximum extent of melting often experienced within a narrow range of dates. Fig. 3c therefore contains microwave radar archaeological evidence for previous melting within the dry snow zone, through the influence of buried scatterers beneath recent years of snow accumulation. Patterns suggest a recent upslope migration of the upper boundary of the percolation zone, particularly in response to the extreme summer of '95 (in Fig. 2e). NSCAT probably penetrates deep enough to 'see' percolation inhomogeneities formed along the lower elevation fringes of the dry snow zone, and the frequency difference image in Fig. 3e corroborates these changes. Fig. 3e highlights zones of wavelength-dependent volume scattering. As dry snow has a lower σ° at C-band, due to the primary backscattering occurring from Rayleigh scattering from snow grains (in the

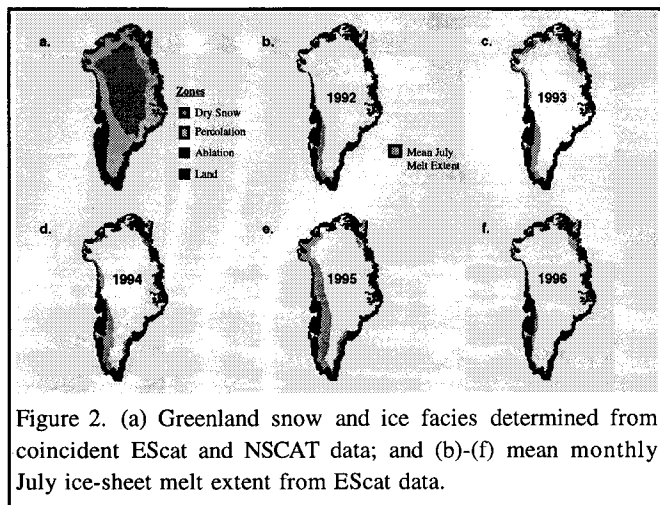


Figure 2. (a) Greenland snow and ice facies determined from coincident EScat and NSCAT data; and (b)-(f) mean monthly July ice-sheet melt extent from EScat data.

values around the lower elevation fringe of the ice sheet, particularly on day 209. The surface-melt signature is similar at both frequencies. Differences in melt extent between the upper and lower panels are accounted for by interannual variability in the length and spatial extent of the melt seasons. Typically, melting ceases by day 237, with refreezing then increasing σ° at both frequencies. Monthly mean July melt extent is shown together with the facies in Fig. 2. The 1990's saw two of the smallest (1992: 8.1×10^4 km²; and 1996: 10.4×10^4 km²), and perhaps the largest (1995: 25×10^4 km²) melt extent in the last two decades. Melting in July 1995 is more extensive than at any other time during the

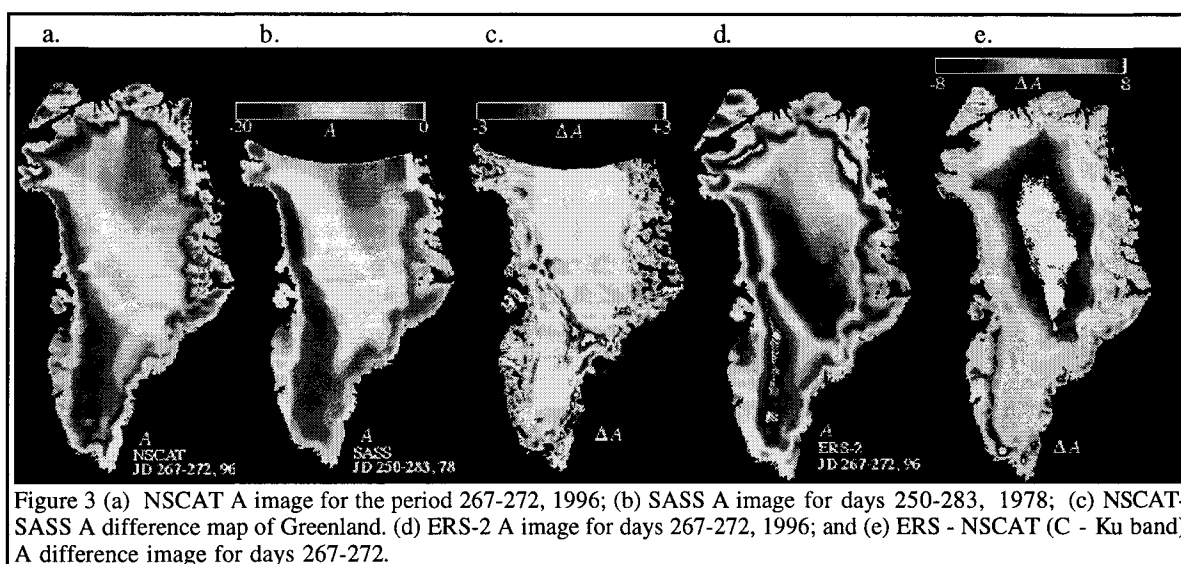


Figure 3 (a) NSCAT A image for the period 267-272, 1996; (b) SASS A image for days 250-283, 1978; (c) NSCAT-SASS A difference map of Greenland. (d) ERS-2 A image for days 267-272, 1996; and (e) ERS - NSCAT (C - Ku band) A difference image for days 267-272.

absence of strong stratigraphy), this zone has large positive values > 8 dB in Fig. 3e. A contrast reversal occurs in the zone influenced by percolation, due to EScat penetrating deeper and responding more to buried ice lenses than NSCAT. This results in slightly negative percolation zone values.

Lower accumulation rates result in more pronounced stratification, and greater backscattering from subsurface layers at high incidence angles. This is particularly true for instance in the north-east dry snow zone, and is seen in SASS data [5]. Thus we suggest that time series of multiple frequency enhanced resolution A images and their associated B values, offer greater potential for retrieving snow accumulation than single channel, fixed incidence angle instrument data. Frequency combinations and the addition of passive microwave emission data from SSM/I help compensate for the wavelength-dependent scattering albedo of the snow and the high incidence angle component of volume backscatter caused by snow grains, as opposed to the stratification induced scattering. This allows dependencies of the backscattering on snow density, temperature, ice particle radius and layer depth to be better parameterized. In this manner, algorithms may be developed to monitor the seasonal progression of snow accumulation and firnification.

CONCLUSIONS

Scatterometers clearly provide important information about the large ice sheets. This spatial and temporal image dataset is complementary to higher resolution sensors such as SAR, and passive microwave images from SSM/I. Time series of images with large-area coverage, such as that shown here, are suitable for monitoring changes in the characteristic zones of ice sheets in response to changes in accumulation and melting. Significant 18 year differences between early NSCAT and Seasat SASS images indicate large-scale changes in radar backscatter in response to changing snow and ice surface conditions.

Decadal variability in Greenland and Antarctica results primarily from the North Atlantic and El Niño Southern Oscillations, respectively. Regional impacts are greater than

normal ablation and/or higher than normal snow accumulation. Our results in Greenland indicate an upslope increase in the extent of the percolation zone and reduction in dry-snow extent since 1978, with the largest changes occurring in the south western flank of the ice sheet. This implies that the region of melting on the ice sheet has risen to its highest altitude in the recent past. Observations of the interannual variability show July 1995 was an extremely large melt season, probably the most significant over the 18 year interval since Seasat in 1978. Changes are consistent with the decadal warming trend and increase of more than 1.0°C between 1979 and the present day.

REFERENCES

- [1] Zwally H.J., A.C. Brenner, Growth of the Greenland Ice Sheet, *Science*, 246, 1587-1591, 1989.
- [2] Abdelati W., K. Steffen, Snowmelt on the Greenland Ice Sheet as Derived from Passive Microwave Satellite Data, *J. Climate*, 10(2), 165-175, 1997.
- [3] Rott H., Synthetic Aperture Radar Capabilities for Glacier Monitoring Demonstrated with Seasat SAR Data, *Z. fuer Gletscherkunde u. Glazialgeol.*, 16, 255-266, 1980.
- [4] Jezek, K.C., M.R. Drinkwater, J.P. Crawford, R. Bindshadler, R. Kwok, Analysis of synthetic aperture radar data collected over the southwestern Greenland ice sheet, *J. Glaciology*, 39, 131, 119-132, 1993.
- [5] Long D.G., M.R. Drinkwater, Greenland Observed at High Resolution by the Seasat-A Scatterometer, *J. Glaciology*, 32, 2, 213-230, 1994.
- [6] Benson C.S., Stratigraphic Studies in the Snow and Firn of the Greenland Ice Sheet, *CRREL Res Rep.*, 70, Cold Regions Res. Eng. Lab., Hanover, NH, 120pp., 1962.
- [7] Rignot, E., Backscatter Model for the Unusual Radar Properties of the Greenland Ice Sheet, *J. Geophys. Res.*, 100, E5, 9389-9400, 1995.
- [8] Jezek, K.C., P. Gogineni, M. Shanableh, *Geophys. Res. Lett.*, 21, 1, 33-36, 1994.
- [9] Drinkwater M.R., D.G. Long, D.S. Early, *ESA Journal* 17, 307-322, 1994.
- [10] Early D.S., D.G. Long, Resolution Enhancement of Scatterometer Data, *IEEE Trans. Geosci. Rem. Sens.*, In Press.